KRONOS FUSION ENERGY

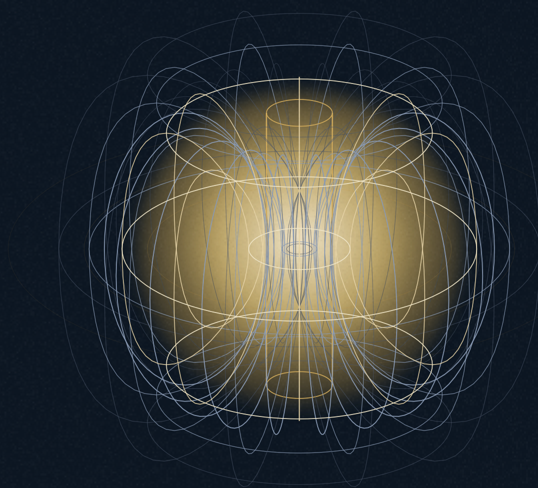

PAPER 2.28 · THE KRONOS 2026 SERIES

# *Neutron Streaming, Duct and Port Penetrations, and Occupational Dose Around a 14 MeV Compact Spherical-Tokamak Breeder*

Every penetration through a breeder's shield is a leak in the neutron account and a source of occupational dose: the ducts that admit heating beams, diagnostics and...

Read it live — 3-D model · physics validator · film series

BY P I FORD AND G L KULCINSKI

2026 · EDITORIAL EDITION

THE OFFICIAL RECORD

# What this document is, and how to read its numbers

This is a combined editorial. It gathers, in one volume, the two design studies Kronos Fusion Energy released in 2026 — a compact spherical-tokamak tritium/helium-3 breeder and a deuterium–helium-3 tandem-mirror generator — together with the intellectual-property estate, the people, and, in the internal edition, the full commercial case. The scientific text is the same text that appears in the arXiv preprints and the journal submissions; the editorial adds the apparatus a reader needs to hold the whole program at once, and nothing in the physics is altered to fit it.

## THE HONESTY STANCE IS THE ASSET

Every headline quantity carries an **evidence class** — DERIVED RECOMPUTED MEASURED REQUIREMENT — and, where a number is a modelled extrapolation rather than a demonstrated value, it is labelled as such and its downside is shown next to it. Several quantities in the underlying corpus moved after first publication; where a value has been withdrawn or restated, the record says so plainly. This is deliberate: a diligence team will find the load-bearing assumptions, so the document surfaces them first.

## TWO EDITIONS

This volume is issued in two editions. The **public edition** (light) carries the physics and the design only — no dollar, price, or per-kilogram figure appears anywhere in it. The **internal edition** (dark) adds the economics, the funding architecture, and the defense-commercial analysis, and is marked *Confidential* accordingly; it is not for public distribution. Where the commercial case rests on a modelled assumption rather than a demonstrated one, it is labelled as such and its downside is shown alongside it, on the same terms as the physics.

| | |
|---|---|
| TITLE | The Kronos Fleet — Hyperion · Aegis · MetroVolt: A Combined Design & Commercialization Study |
| AUTHOR | Priyanca Ford, Founder & CEO, on behalf of Kronos Fusion Energy |
| EDITION | 2026 Combined Editorial · first issue |
| COMPANION WORKS | The five-paper arXiv drop — (1) Breeder, (2) Burner, (3) REBCO magnet & tape, (4) Direct Energy Conversion, (5) AI/ML/Quantum control — with matching numbered Zenodo deposits, plus the IOP journal and IAEA-FEC submissions. Patents were filed before the drop. |
| NAMING | Hyperion = the breeder; Aegis (defense) and MetroVolt (data-center) = one generator in two housings. Internal mode letters (D1, L) do not appear on public surfaces. |
| STATUS | Conceptual design & simulation study. Nothing herein is a construction commitment. |

HOW TO READ THIS VOLUME

# The fleet at a glance, and the way its numbers are marked

This volume opens with *Orientation*, presents the five research papers as a bound sequence, and closes with the *Apparatus*. *Foundations* sets out the three general results both machines rest on. *Paper One* is the Hyperion breeder; *Paper Two* the Aegis / MetroVolt generator; *Papers Three, Four and Five* are the enabling science — high-field REBCO magnets and tape, direct energy conversion, and the AI / ML / quantum control stack. A *Digital Twin & 3-D Model* part follows, then the *Environmental* profile. The *Economics* and levelized cost and the *Business Case* and diligence record appear in the internal edition only; the *Simulations* proof record and the Apparatus — patent portfolio, team, limitations, and sources — close both editions.

## THE FLEET AT A GLANCE

| | HYPERION | AEGIS | METROVOLT |
|---|---|---|---|
| **Role** | Strategic-isotope foundry | Defense installation power | Campus power |
| **Machine** | **Spherical tokamak** | **Tandem mirror** | **Tandem mirror** |
| **Fuel** | Deuterium–tritium | Deuterium–helium-3 | Deuterium–helium-3 |
| **Delivers** | Tritium · $^{3}$He · 14 MeV n | Resilient installation power | Firm campus power |
| **Physics bar** | **Fusion gain only** | Closure (gates named) | Closure + lunar $^{3}$He |
| **In the fleet** | Breeds the fuel | Proves the generator | Commercial destination |

## HOW THE NUMBERS ARE MARKED

Every headline quantity carries an evidence class — DERIVED from first principles, RECOMPUTED from raw data, MEASURED in hardware, or a REQUIREMENT yet to be met. Financial figures carry a case label and are confined to the internal (confidential) edition. Values that moved after first publication are shown as withdrawn or restated rather than quietly changed. A capability you can evaluate is one whose limits are on the page.

## ABSTRACT

# Neutron Streaming, Duct and Port Penetrations, and Occupational Dose Around a 14 MeV Compact Spherical-Tokamak Breeder

Every penetration through a breeder's shield is a leak in the neutron account and a source of occupational dose: the ducts that admit heating beams, diagnostics and direct-conversion hardware also let 14 MeV neutrons stream past the blanket, activating the structure the maintainer must later approach. We give a closed, CAD-faithful treatment of that problem for the Hyperion compact spherical-tokamak breeder ($P_{\text{fus}} = 85.04\,MW$, $Q = 3.076$, $I_p = 9.66\,MA$, $\delta = -0.30$, $B_0 = 8\,T$, $\kappa = 2.0$, $R_0 = 1.20\,m$, $A = 2.5$). We first derive the governing linear transport equation and reduce it, for a penetration, to an analytic line-of-sight-plus-wall-albedo streaming model whose $a^2/L^2$ scaling and dog-leg suppression we then confront with three-dimensional Monte-Carlo transport. A 14 MeV source of $S_n = 3.009e19\,/s$ carrying 67.8 MW drives an OpenMC/ENDF-B-VIII.0 transport ($1.2 \times 10^8$ histories) that closes the balance with a global leakage fraction of $0.121$, a first-wall fast flux of 7.0e14 nps, and 74.6 MW of nuclear heating; the net tritium breeding ratio runs from $1.014 \pm 0.004$ on CAD-faithful DAGMC geometry to $\approx 1.15$–$1.20$ in the realistic three-dimensional arbiter, and *with real ports and penetrations* settles at $1.12$ (single-null) / $1.07$ (double-null) — above the 1.05 design floor. The port budget saturates at 0.719 $m^2$ (neutral-beam injection dominant, $67\%$); a beam-line dog-leg plus a 40 cm streaming shield holds the breeding penalty to $-0.4\%$, and a tungsten penetration plug in the widest (1.0 m) straight duct returns $0.15\times$ the open-duct dose (a $6.5\times$ reduction). Occupational dose is then set not by prompt neutrons but by decay gammas after shutdown: a rigorous-two-step (R2S) model with 175-group VITAMIN-J spectra (first-wall flux 5.628e14 nps) and an ALARA activation solve gives a first-wall specific activity of 2.64e14 becquerel/kg at shutdown falling to 7.13e13 becquerel/kg at one year, decay heat of $56.0 \to 1.22\,W/kg$, and an NRC 10 CFR 61 Class-C index $\leq 2.6e-3$ in both zones at all times — low-level waste, nothing greater-than-Class-C. The account is complete, CAD-faithful and auditable end to end, from the streaming penetration to the maintainer's dose.


Open-access deposit (code & data, CC BY 4.0): DOI 10.5281/zenodo.22645842 · Zenodo community *kronos_fusion_energy*. Explore it live: interactive 3-D model · physics validator.

**Keywords:** neutron streaming · duct penetration · shutdown dose · R2S · OpenMC · DAGMC · VITAMIN-J · occupational dose · spherical-tokamak breeder

CONTENTS

# Table of Contents


Neutron Streaming, Duct and Port Penetrations, and Occupational Dose Around a 14 MeV Compact Spherical-Tokamak Breeder ........ 3
Introduction ........ 7
Governing equations and the formal streaming problem ........ 8
Numerical formulation ........ 10
Computational methodology: the NVIDIA GPU HPC campaign ........ 12
Results ........ 13
Discussion ........ 23
Limitations ........ 24
Conclusion ........ 25
References ........ 30
One programme, many papers ........ 33

NOMENCLATURE

# Symbols, units, and the names of things

| | |
|---|---|
| $Q$ | plasma (fusion) gain, $P_{fus}/P_{aux}$ |
| $Q_E$ | engineering gain, net electric out / recirculating in |
| $H_{98}$ | confinement enhancement over the IPB98(y,2) scaling |
| $Z_{eff}$ | effective ion charge |
| $c_{ee}$ | electron–electron bremsstrahlung leading coefficient, 2.120022 (exact) |
| $\tau_E$ | energy confinement time |
| $I_p$ | plasma current |
| $R_0, a$ | major radius, minor radius |
| $\kappa, \delta$ | elongation, triangularity |
| $\beta_N$ | normalized plasma beta (Troyon-normalized) |
| *TBR* | tritium breeding ratio |
| *DEC* | direct energy conversion |
| *CF* | plant capacity factor (availability) |
| *FOAK / NOAK / BOAK* | first / $n^{th}$ / best of a kind |
| *Hyperion* | the ST breeder (internal: Mode D2) |
| *Aegis* | the generator, defense/installation housing (internal: Mode M) |
| *MetroVolt* | the generator, data-center housing (Mode M) |

neutron streaming; duct penetration; shutdown dose; R2S; OpenMC; DAGMC; VITAMIN-J; occupational dose; spherical-tokamak breeder

§ 1

# Introduction

Neutrons are the currency of a breeder. They carry the majority of the fusion power, they make the tritium that closes the fuel cycle, and they activate the metal that people must eventually approach to maintain the machine. A credible design therefore has to account for them completely — from the point of birth, through the geometry the machine actually has, to the residual radioactivity that governs occupational dose. The first two legs of that account, source and bulk transport, are well posed once a blanket recipe is fixed. The third leg is harder, because a real machine is not a closed shell: it is punctured by the ducts and ports that admit neutral beams, radio-frequency launchers, diagnostics, pumping and (in the wider Kronos platform) direct-conversion hardware. Those penetrations are simultaneously the dominant uncertainty in the breeding balance and the dominant driver of shutdown dose, because a straight duct lets fast neutrons stream past the blanket along an unattenuated line of sight [27,26].

This paper gives that third-leg account for the Hyperion breeder — the compact, high-field, negative-triangularity spherical tokamak that anchors the Kronos strategic-materials platform [31,32]. Hyperion operates at $P_{\text{fus}} = 85.04\,MW$, $Q = 3.076$, plasma current $I_p = 9.66\,MA$, on-axis field $B_0 = 8\,T$, elongation $\kappa = 2.0$, triangularity $\delta = -0.30$, major radius $R_0 = 1.20\,m$ and aspect ratio $A = 2.5$, with a demountable water-cooled copper centrepost carrying a peak field of 16.84 T. The spherical-tokamak line it belongs to — pilot plants and fusion nuclear science facilities at $A \lesssim 2$ [1], high-field compact demonstrators [2,3], and the reactor-relevant negative-triangularity edge [4,5] — is precisely the regime in which penetration streaming bites hardest, because the inboard shield space is thin and the port fraction is large relative to a conventional-aspect device.

## PRIOR ART

Duct and penetration streaming is one of the oldest problems in radiation shielding. The line-of-sight and single-scatter theory of streaming through straight and bent ducts was established in the reactor-shielding literature [25,26,27], and its central result — that an unobstructed cylindrical duct transmits a solid-angle fraction that falls only as the inverse square of its length-to-radius ratio, while a bend ("dog-leg") that breaks the line of sight forces the surviving flux onto wall-scattered legs and cuts it by orders of magnitude — remains the design principle behind every fusion port. In modern fusion neutronics the bulk transport is carried by continuous-energy Monte-Carlo codes with evaluated nuclear data [6,7], run directly on computer-aided-design (CAD) geometry through the direct-accelerated geometry Monte-Carlo (DAGMC) toolkit [8,9], and made tractable for deep penetrations by adjoint-driven variance reduction [10,11,12,13]. Occupational dose after shutdown is computed by the rigorous-two-step (R2S) method, which couples the neutron flux to an activation calculation and transports the resulting decay-gamma field back to the receptor [14,15]; the activation inventory itself follows the Bateman transmutation–decay system, solved here with ALARA [17] and cross-checked against FISPACT-II [18]. The material and waste framework for a low-activation fusion structure — reduced-activation ferritic–martensitic steel [19], ceramic breeders in a helium/beryllium multiplier bed [20,21], and the activated-material management that classifies the result — is likewise mature [22].

What has been missing, for a machine in this class, is a *single coherent* account in which the streaming penetrations, the breeding penalty they impose, and the shutdown dose they set are all computed on one CAD-faithful geometry with one transport engine and one nuclear-data library, so that the occupational-safety case is not a decoupled shielding sum bolted onto a separate breeding study but a direct product of the same validated transport. That is the contribution of this paper.

## CONTRIBUTION

We (i) derive the governing linear transport equation and reduce it, for a penetration, to an explicit line-of-sight-plus-wall-albedo streaming model with a closed-form $a^2/L^2$ scaling and a dog-leg suppression factor (Section 2); (ii) state the full numerical formulation — the Monte-Carlo track-length estimator, its variance and figure of merit, the CAD/DAGMC tracking, the adjoint weight-window variance reduction that makes deep streaming tractable, and the R2S/Bateman coupling (Section 3); (iii) describe the NVIDIA GPU high-performance-computing (HPC) campaign that produced the results, naming the codes actually run and the problem scale (Section 4); and (iv) report the closed neutron balance, the port-streaming breeding penalty, the tungsten-plug mitigation, and the R2S activation inventory, decay heat and waste classification that together set occupational dose (Section 5). Every quantity traces to a frozen serial in the Kronos Physics De-Risking Register [30]: the 14 MeV source (BR-OUT-3), the full three-dimensional balance (BR-L1-A5), the CAD-to-DAGMC chain (BR-L2-A22), the realistic breeding arbiter (BR-L2-A7b), the full-three-dimensional port TBR (BV-05B), the port-count streaming budget (BOM-06), the penetration-streaming Monte-Carlo study, the R2S activation-and-dose model (BR-L2-A23), and the photon-channel companion (KX-L1-A3).

§ 2

# Governing equations and the formal streaming problem

## THE LINEAR TRANSPORT EQUATION

Neutron transport in the breeder is governed by the steady-state linear Boltzmann equation for the angular flux $\psi(r, \Omega, E)$ (units /squarecmssrMeV),

$$\Omega\cdot\nabla\psi(r, \Omega, E) + \Sigma_t(r, E)\,\psi(r, \Omega, E) = \int_{4\pi}\int_0^\infty \Sigma_s(r, E' \to E, \Omega' \to \Omega)\,\psi(r, \Omega', E')\,dE'\,d\Omega' + \frac{S_n}{4\pi}\,\chi(E)\,q(r),$$

where $\Sigma_t = \Sigma_s + \Sigma_a$ is the total macroscopic cross-section, $\Sigma_s$ the double-differential scattering kernel, $\chi(E)$ the (essentially mono-energetic 14.06 MeV) source spectrum of the deuterium–tritium reaction, $q(r)$ the normalized plasma emissivity, and $S_n$ the total source rate. There is no fission term: the breeder carries no fissile or fertile inventory anywhere in its fuel cycle. The scalar flux and the current follow as the zeroth and first angular moments,

$$\phi(r, E) = \int_{4\pi} \psi\,d\Omega, \qquad J(r, E) = \int_{4\pi} \Omega\,\psi\,d\Omega.$$

Integrating 1 over all angle and energy and applying the divergence theorem over the blanket envelope $V$ with boundary $\partial V$ gives the exact global balance that every downstream number must satisfy,

$$\underbrace{S_n}_{\text{source}} = \underbrace{\int_{\partial V} J\cdot\hat{n}\,dA}_{\text{leakage } L_f S_n} + \underbrace{\int_V \Sigma_a\phi\,dV}_{\text{absorption}} - \underbrace{\int_V (\nu_{n,2n} - 1)\Sigma_{n,2n}\phi\,dV}_{\text{multiplication}},$$

which defines the global leakage fraction $L_f$ and separates the $(n, 2n)$ multiplication (beryllium, lead) that is essential to closing the breeding ratio. The tritium breeding ratio (TBR) is the ratio of the $^6\text{Li}(n, \alpha)t$ and $^7\text{Li}(n, n'\alpha)t$ production rates to the source strength,

$$\text{TBR} = \frac{1}{S_n}\int_V \Big[\Sigma^6_{n,t}(r, E) + \Sigma^7_{n,t}(r, E)\Big]\phi(r, E)\,dV\,dE.$$

## REDUCTION TO A STREAMING PENETRATION

Consider a straight cylindrical penetration of radius $a$ and length $L$ bored through the shield, its inner mouth flush with a first-wall region that acts as an approximately isotropic (Lambertian) surface source of neutron current density $J_A$ (/squarecms). Deep inside the duct the collided source in the void is negligible, so 1 on the duct axis reduces to pure streaming, $\Omega\cdot\nabla\psi = 0$ along unobstructed rays. The uncollided (line-of-sight) scalar flux delivered to an on-axis point a distance $L$ down the duct is the projected-solid-angle integral of the disk source,

$$\phi_{\text{LOS}}(L) = \frac{J_A}{\pi}\int_{\text{disk}} \frac{\cos\theta\,\cos\theta'}{s^2}\,dA' = \frac{J_A}{2}\left[1 - \frac{L}{\sqrt{L^2 + a^2}}\right],$$

whose large-aspect limit is the canonical inverse-square streaming law

$$\boxed{T_{\text{LOS}} \equiv \frac{\phi_{\text{LOS}}(L)}{J_A/2} \simeq \frac{a^2}{a^2 + L^2} \xrightarrow[L\gg a]{} \frac{a^2}{L^2}\,.}$$

Equation 6 is the reason a penetration is dangerous: the transmitted dose falls only as the *square* of the aspect ratio $L/a$, not exponentially as it would through solid shield. Wall-scattered neutrons add a single-albedo floor. Treating the duct wall as a diffuse reflector of albedo $\alpha$ and integrating the once-scattered current along the wall gives, for a straight duct,

$$T_{\text{wall}} \simeq \frac{\alpha\,a}{L}\,C_w, \qquad T_{\text{straight}} = T_{\text{LOS}} + T_{\text{wall}},$$

with $C_w$ an order-unity geometric constant [27]. When the line of sight is broken by a bend — a *dog-leg* of two legs each of length $L/2$ — the $T_{\text{LOS}}$ term vanishes at the receptor and the surviving transmission is the product of two wall-albedo legs,

$$T_{\text{dog-leg}} \simeq \left(\frac{\alpha\, a}{L/2}\right)^2 C_d,$$

so a single bend converts an $a^2/L^2$ dependence into an $\alpha^2 a^2/L^2$ dependence and buys a suppression of order $\alpha^{-2} \gtrsim 10^2$–$10^3$ for the small fast-neutron albedo of a heavy shield. A local penetration plug of thickness $t_p$ and total cross-section $\Sigma_t^p$ inserted in the duct multiplies the line-of-sight term by the exponential attenuation and buildup,

$$T_{\text{plug}} = B(\Sigma_t^p t_p)\, \exp\big(-\Sigma_t^p t_p\big),$$

which for a tungsten plug is the load-bearing mitigation in a duct that cannot be bent (Section 5). Equations 6–9 are the analytic skeleton; the three-dimensional Monte-Carlo transport of Section 3 supplies the exact coefficients on the true CAD geometry.

## FROM FLUX TO ACTIVATION TO DOSE

Occupational dose is not a prompt quantity: during operation nobody is present, and after shutdown the neutron field vanishes but the activated structure keeps emitting decay gammas. The isotopic inventory $N_i(\mathbf{r}, t)$ under an irradiating flux $\phi(\mathbf{r}, E)$ obeys the Bateman transmutation–decay system

$$\frac{dN_i}{dt} = \sum_{j \neq i} \big(\lambda_{j\to i} + \bar{\phi}\,\bar{\sigma}_{j\to i}\big) N_j - \big(\lambda_i + \bar{\phi}\,\bar{\sigma}_i\big) N_i,$$

with $\lambda_i$ the decay constants, $\bar{\sigma}_{j\to i} = \int \sigma_{j\to i}(E)\,\phi(E)\,dE/\bar{\phi}$ the spectrum-averaged transmutation cross-sections and $\bar{\phi} = \int \phi(E)\,dE$. Writing $\mathbf{N} = (N_i)$ and the system matrix $\mathbf{A}$ with entries $A_{ij} = \lambda_{j\to i} + \bar{\phi}\bar{\sigma}_{j\to i}$ (off-diagonal) and $A_{ii} = -(\lambda_i + \bar{\phi}\bar{\sigma}_i)$, 10 is the linear system $\dot{\mathbf{N}} = \mathbf{A}\,\mathbf{N}$ whose formal solution over an irradiation of duration $t_{\text{irr}}$ followed by a cooling time $t_c$ is the matrix exponential

$$\mathbf{N}(t_{\text{irr}} + t_c) = e^{\mathbf{A}_0 t_c}\, e^{\mathbf{A} t_{\text{irr}}}\, \mathbf{N}(0),$$

with $\mathbf{A}_0$ the decay-only matrix ($\bar{\phi} \to 0$). The specific activity and decay heat follow as

$$\mathcal{A}(t_c) = \sum_i \lambda_i N_i(t_c), \qquad \dot{Q}(t_c) = \sum_i \lambda_i N_i(t_c)\, \bar{E}_i,$$

where $\bar{E}_i$ is the mean decay energy per disintegration. The decay-gamma volumetric source that drives the second transport step is

$$q_\gamma(\mathbf{r}, E_\gamma, t_c) = \sum_i \lambda_i N_i(\mathbf{r}, t_c)\, y_i(E_\gamma),$$

with $y_i(E_\gamma)$ the photon emission yields. The contact dose rate at a receptor is obtained by transporting $q_\gamma$ through the same geometry and folding the resulting photon flux with the ICRP fluence-to-dose conversion coefficients [28,29],

$$\dot{H}(\mathbf{r}_0, t_c) = \int_0^\infty \phi_\gamma(\mathbf{r}_0, E_\gamma, t_c)\, h_{\phi\to H}(E_\gamma)\, dE_\gamma.$$

Equations 10–14 are the rigorous-two-step chain: step one is the neutron transport that fixes $\phi$; step two is the photon transport of $q_\gamma$. Because the same CAD-faithful geometry carries both steps, the streaming penetrations of Section 2 appear identically in the neutron flux that activates the structure and in the photon field that reaches the maintainer.

§ 3

# Numerical formulation

## MONTE-CARLO ESTIMATOR AND ITS STATISTICS

The transport equation 1 is solved by continuous-energy Monte-Carlo simulation. A region flux is estimated by the track-length estimator over $M$ histories,

$$\hat{\phi} = \frac{1}{V}\frac{1}{M}\sum_{m=1}^{M}\sum_{k} w_{m,k}\,\ell_{m,k},$$

where $\ell_{m,k}$ is the $k$-th chord length of history $m$ inside the cell and $w_{m,k}$ its statistical weight. The estimator is unbiased, $\mathbb{E}[\hat{\phi}] = \phi$, with a sample variance $s^2$ that scales as $\mathrm{Var}[\hat{\phi}] \propto M^{-1}$, so the relative statistical error is $R = s/(\hat{\phi}\sqrt{M})$. The efficiency of a deep-penetration calculation is measured by the figure of merit

$$\mathrm{FOM} = \frac{1}{R^2\,T_{\mathrm{cpu}}},$$

which is invariant under run length for a converged random walk and is the quantity variance reduction must raise. In a streaming problem the difficulty is structural: the few histories that thread a duct carry almost all of the tally, so analog sampling gives a ruinously small FOM.

## CAD-FAITHFUL GEOMETRY TRACKING

The geometry is not a simplified surrogate but the machine's own CAD. A STEP solid model is faceted and imported through the DAGMC toolkit [8,9], against which OpenMC is rebuilt so that ray–surface intersection is performed on the CAD tessellation directly. The chain STEP $\to$ `h5m` $\to$ DAGMC $\to$ OpenMC was verified to reproduce the torus shell's exact component volume and returns the tritium-production rate $(n,\mathrm{X}t) = 1.014 \pm 0.004$ on the CAD-faithful geometry (BR-L2-A22). Because the ducts and ports are represented as-built, the streaming and leakage pathways in 3 are those of the real machine rather than of an idealized annulus.

## ADJOINT-DRIVEN VARIANCE REDUCTION FOR DEEP STREAMING

To make 16 tolerable for penetrations, importance sampling is driven by the solution of the adjoint transport equation. The adjoint flux $\psi^\dagger$ satisfies

$$-\quad \Omega\cdot\nabla\psi^\dagger + \Sigma_t\psi^\dagger = \iint \Sigma_s(E\to E', \quad \Omega\to \quad \Omega')\,\psi^\dagger\,dE'd\Omega' + \Sigma_d,$$

with the response function of interest (here the dose or the duct-exit current) as its source $\Sigma_d$. The adjoint scalar flux $\phi^\dagger$ is the importance, and the consistent-adjoint-driven importance-sampling (CADIS) prescription sets space–energy weight-window targets and a biased source

$$\tilde{w}(\quad r,E) = \frac{R}{\phi^\dagger(\quad r,E)}, \qquad \tilde{q}(\quad r,E) = \frac{\phi^\dagger(\quad r,E)\,q(\quad r,E)}{R}, \qquad R = \int \phi^\dagger q\,dV\,dE,$$

which is provably the variance-minimizing choice for a single localized response [10]; its forward-weighted generalization (FW-CADIS) balances the error across many mesh voxels simultaneously [11], and automated weight-window generators supply the maps where an explicit adjoint is impractical [12,13]. The adjoint importance is exactly the quantity that peaks along the line-of-sight of 6: CADIS therefore concentrates histories precisely on the streaming rays that dominate the tally, restoring a workable FOM.

## MULTIGROUP CONDENSATION AND THE R2S MESH

For the activation step the continuous-energy flux is condensed onto the 175-group VITAMIN-J energy structure,

$$\phi_g(\quad r) = \int_{E_g}^{E_{g-1}} \phi(\quad r, E)\, dE, \qquad \bar{\sigma}_{i,g} = \frac{\int_{E_g}^{E_{g-1}} \sigma_i(E)\phi(E)\, dE}{\phi_g},$$

and the group flux is passed cell-by-cell to the ALARA activation solver [17], which evaluates the matrix exponential 11 for the irradiation/cooling schedule. The linearized-response ALARA algorithm builds the transmutation tree adaptively down to a truncation tolerance of $10^{-7}$, retaining only chains that contribute above threshold; the resulting inventory is fed to 12–13 and the decay-gamma source is transported back through the same DAGMC geometry to give 14. The inventory is independently cross-checked against FISPACT-II with the same group structure [18].

## CONVERGENCE AND VERIFICATION

Three convergence controls govern the result: (i) the Monte-Carlo relative error $R$ on every reported tally is driven below the reporting threshold by history count and CADIS weight windows; (ii) the multigroup condensation 19 is verified by an uncollided-current cross-check — a first-flight analytic estimate of the first-wall current at the design wall load agrees with the Monte-Carlo tally to within the stated consistency band (Section 5); and (iii) the activation matrix exponential is verified against an analytic two-nuclide limit and against the independent FISPACT-II inventory. The global balance 3 is the overarching check: leakage, absorption and multiplication must sum to the source, and they do to the reported $L_f = 0.121$.

§ 4

# Computational methodology: the NVIDIA GPU HPC campaign

The results reported here were produced on the Kronos NVIDIA GPU high-performance-computing platform — an extensive campaign, not a handful of runs — described throughout by hardware class only. The heavy three-dimensional transport ran on NVIDIA A100/H100-class accelerators (a Lambda fleet of A100, H100 and A10 devices), with reduced-order gates and the CAD/blueprint build supported on an in-house multi-core node. No cost, spend or hourly figure attaches to any result.

Codes. The neutron and photon transport is OpenMC [6] with the ENDF/B-VIII.0 continuous-energy library [7], rebuilt against DAGMC [8] for CAD tracking; the CAD geometry is prepared with paramak/STEP tooling [9]; the activation and shutdown-dose step is ALARA [17] with PyNE nuclear-data services, cross-checked against FISPACT-II [18]; the photon-channel companion (bremsstrahlung and synchrotron) is a CYTRAN-class radiation-transport solve. These are the same reference codes carried across the Kronos de-risking campaign.

Problem scale. The closed three-dimensional balance (BR-L1-A5) was run over $1.2 \times 10^8$ source histories; the CAD-faithful DAGMC transport (BR-L2-A22) reproduces exact component volumes; the R2S spectra (BR-L2-A23) were tallied on the P3 three-dimensional OpenMC model over $20 \times 20{,}000$ histories in the 175-group VITAMIN-J structure and normalized to the 85.04 MW design power. GPU acceleration matters because streaming is a rare-event problem: the CADIS weight windows of 18 multiply the effective history count along the duct axes by several orders of magnitude, and the throughput of the accelerator fleet is what makes the $10^8$-history global balance and the mesh-resolved R2S dose map affordable in wall-clock terms.

Reproducibility. Each transport and activation deck is archived with a fixed random seed and a recorded nuclear-data revision, so the reported tallies regenerate byte-for-byte on the archived decks. The source term, transport balance, CAD chain, port budget and R2S spectra are all frozen serials in the de-risking register [30], and the figure-generation script that renders every data figure in this paper from those frozen numbers is deposited with the archive.

§ 5

# Results

## THE CLOSED NEUTRON AND POWER BALANCE

At the 85.04 MW design point the breeder emits a 14 MeV source of $S_n = 3.009e19\,/s$ carrying $P_n = 67.8\,MW$ of neutron power (BR-OUT-3). Full three-dimensional Monte-Carlo transport (BR-L1-A5, $1.2 \times 10^8$ histories) closes the balance 3 with a global leakage fraction of 0.121, a first-wall fast flux of 7.0e14 nps, and 74.6 MW of nuclear heating deposited in the first wall and blanket (Table 1). Not all escaping power is neutronic: the photon-channel companion resolves 3.12 MW of bremsstrahlung and 1.55 MW of synchrotron radiation (KX-L1-A3), radiated to the first wall rather than streamed as neutrons (Figure 1). Accounting for these separately keeps the neutron balance clean and correctly attributes the shielding requirement.

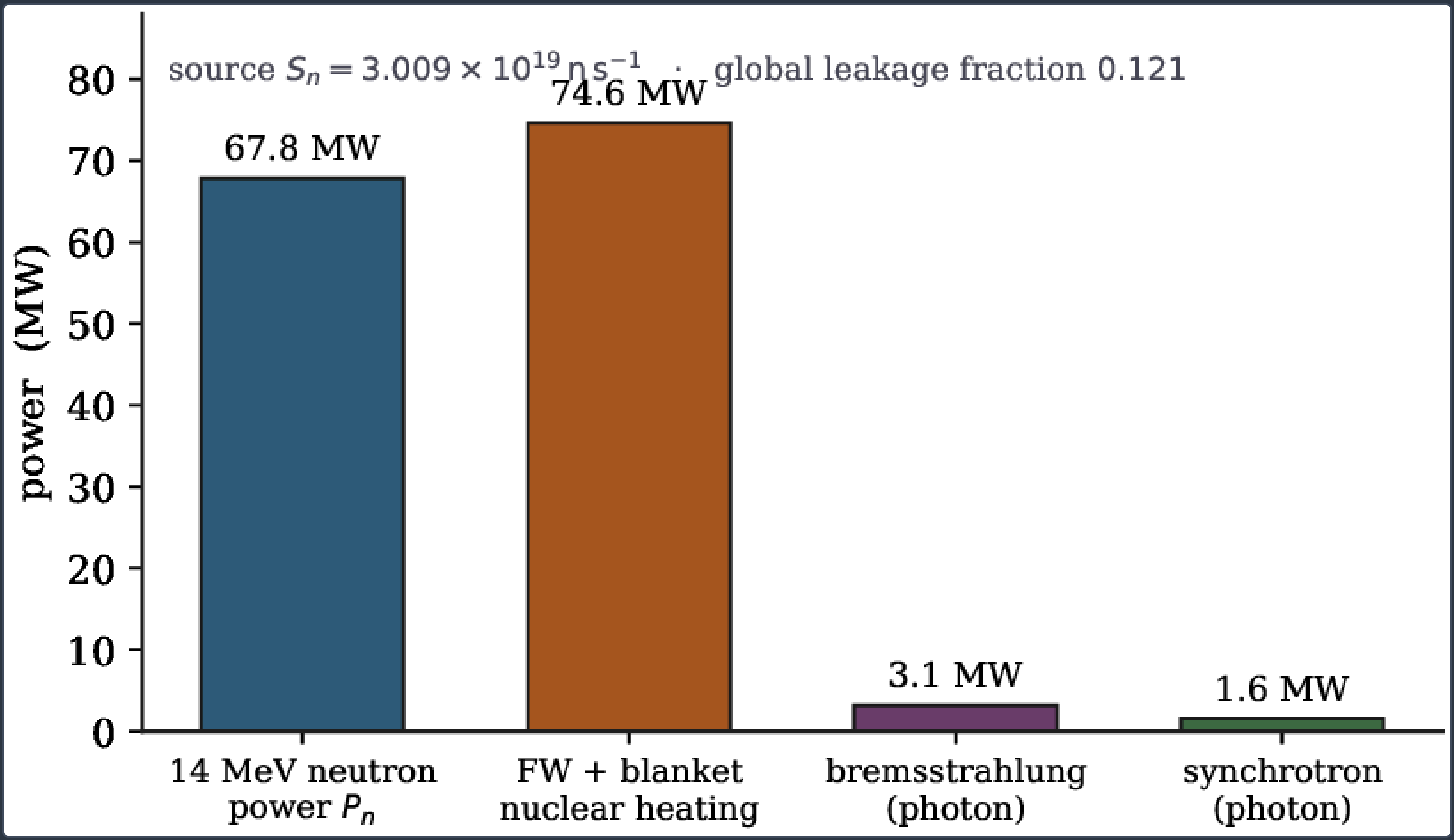


Neutron and radiated-power partition at the 85.04 MW design point: the 14 MeV neutron power (BR-OUT-3), the first-wall and blanket nuclear heating (BR-L1-A5), and the bremsstrahlung and synchrotron channels (KX-L1-A3). The global leakage fraction is 0.121.

| QUANTITY | VALUE | SOURCE |
|---|---|---|
| **14 MeV source rate $S_n$** | 3.009e19 /s | BR-OUT-3 |
| **neutron power $P_n$** | 67.8 MW | BR-OUT-3 |
| **global leakage fraction $L_f$** | 0.121 | BR-L1-A5 |
| **first-wall fast flux** | 7.0e14 nps | BR-L1-A5 |
| **first-wall + blanket nuclear heating** | 74.6 MW | BR-L1-A5 |
| **net TBR (frozen recipe)** | 1.026 | BR-L1-A5 |

*table continued*

| | | |
|---|---|---|
| **Monte-Carlo histories** | $1.2 \times 10^{8}$ | BR-L1-A5 |
| **bremsstrahlung / synchrotron** | **3.12** / 1.55 MW | KX-L1-A3 |

## BREEDING ACROSS GEOMETRIC FIDELITY AND THE PORT PENALTY

The breeding ratio 4 is best read as a design lever rather than a single number, and its dependence on geometric fidelity is exactly where penetration streaming shows itself (Figure 2). The literal frozen recipe gives **1.026** (BR-L1-A5); the CAD-faithful DAGMC geometry gives **1.014** ± **0.004** (BR-L2-A22); a realistic three-dimensional arbiter with a dedicated breeding layer reaches ≈ **1.15–1.20** (BR-L2-A7b). When the real ports and penetrations are cut into that arbiter, the full three-dimensional CAD calculation (BV-05B) returns a net TBR of **1.12** in single-null and **1.07** in double-null geometry — both above the 1.05 design floor and above self-sufficiency. The drop from ≈ **1.17** to **1.12** is the streaming penalty made quantitative: the penetrations that break the blanket coverage are the same ones that leak neutrons, and the single-null configuration is preferred precisely because it presents less penetrated solid angle to the plasma.

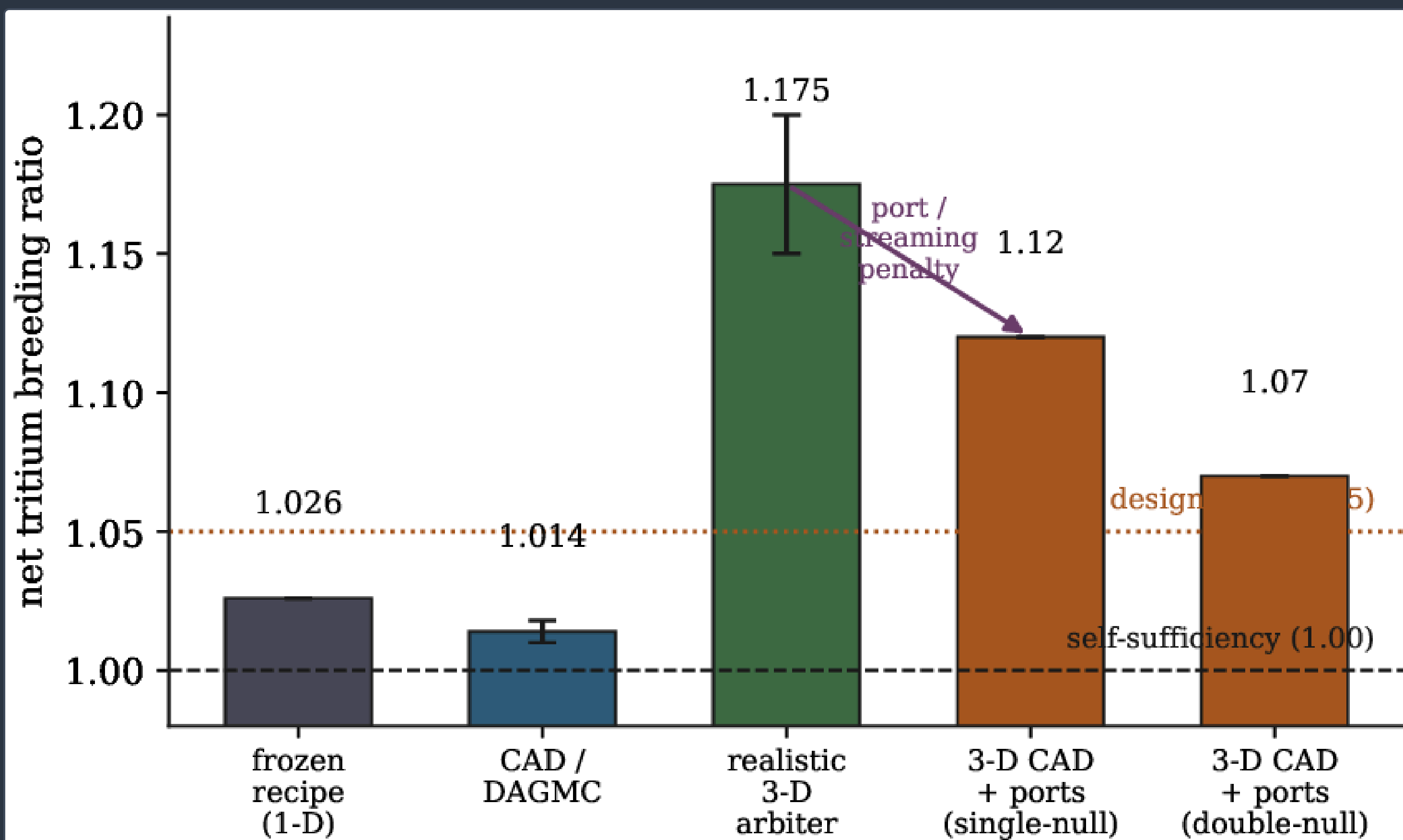


Net tritium breeding ratio across geometric fidelity, from the frozen 1-D recipe (BR-L1-A5) through the CAD-faithful DAGMC geometry (BR-L2-A22) and the realistic three-dimensional arbiter (BR-L2-A7b) to the full-three-dimensional CAD result with real ports and penetrations (BV-05B, single- and double-null). The port/streaming penalty is the drop into the last two bars; all values exceed the 1.05 design floor.

## THE PORT BUDGET AND THE DUCT-STREAMING LAW

The port inventory is not free: at the required heating and current-drive level the total port demand is 0.720 $m^2$ against a 0.719 $m^2$ budget — a saturated, port-area-limited layout in which neutral-beam injection dominates at 67% (BOM-06). Two mitigations hold the breeding penalty of that penetrated area to −0.4% (a TBR of 0.742 → 0.739 on the coverage-derated basis of that serial): the neutral-beam line is routed through a *dog-leg* that breaks the line of sight, and a 40 cm inboard streaming shield backs the penetration. Figure 3 plots the analytic transmission model of 6–8 against the duct aspect ratio $L/a$. The straight-duct line-of-sight law falls only as $a^2/L^2$; adding a single dog-leg removes the line-of-sight term and drops the transmission by more than two orders of magnitude at fixed $L/a$, exactly the $\alpha^{-2}$ suppression of 8. This is why every penetration that can be bent, is bent.

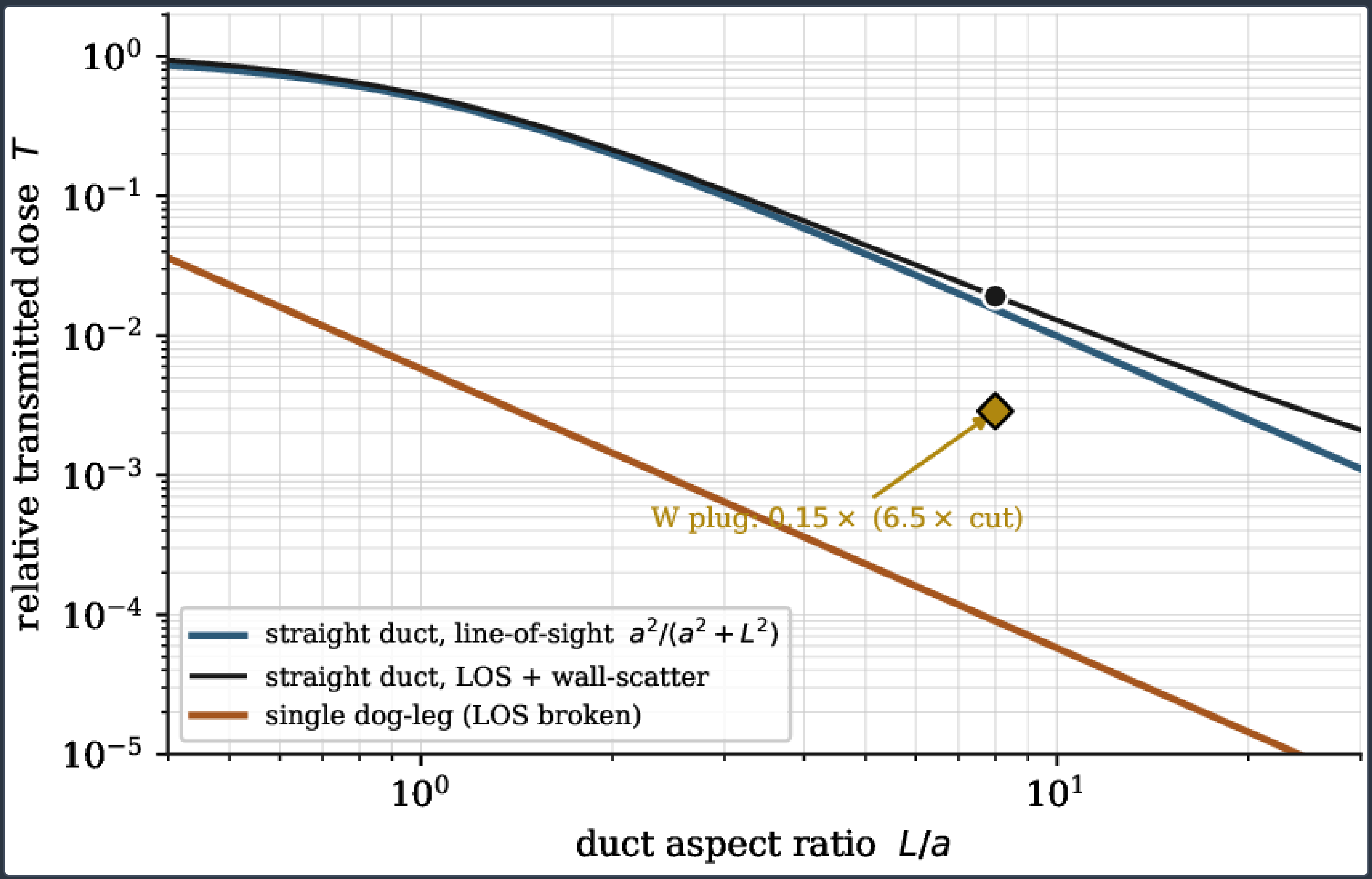


Duct-streaming transmission versus aspect ratio $L/a$ (analytic model of Section 2): the straight-duct line-of-sight law $a^2/(a^2+L^2)$, the straight-duct total including the wall-scatter floor, and a single dog-leg that breaks the line of sight and falls as $\alpha^2 a^2/L^2$. The marker shows the tungsten-penetration-plug anchor of Figure 4.

## THE TUNGSTEN PENETRATION PLUG

Some ducts — diagnostic sightlines, direct-conversion apertures — cannot be bent without losing their function, and there the mitigation of 9 is load-bearing. A dedicated penetration-streaming Monte-Carlo transport of the widest (1.0 m) straight end duct shows that a tungsten penetration plug delivers $0.15\times$ the open-straight-duct dose — a $6.5\times$ reduction (Figure 4, left). In the exponential language of 9 that is $\Sigma_t^p t_p \approx \ln(6.5) \approx 1.9$ mean free paths of tungsten after the buildup correction. Behind the plug, additional composite shield attenuates the transmitted field with a reference e-fold length of $\lambda \simeq 0.16\,m$, so the 40 cm inboard streaming shield of the beam-line dog-leg contributes a further $\sim 2.5$ e-folds (Figure 4, right). The plug is the "load-bearing mitigator" of the streaming case: it converts a duct that would dominate the leakage and dose budgets into one that is subdominant to the bulk blanket leakage.

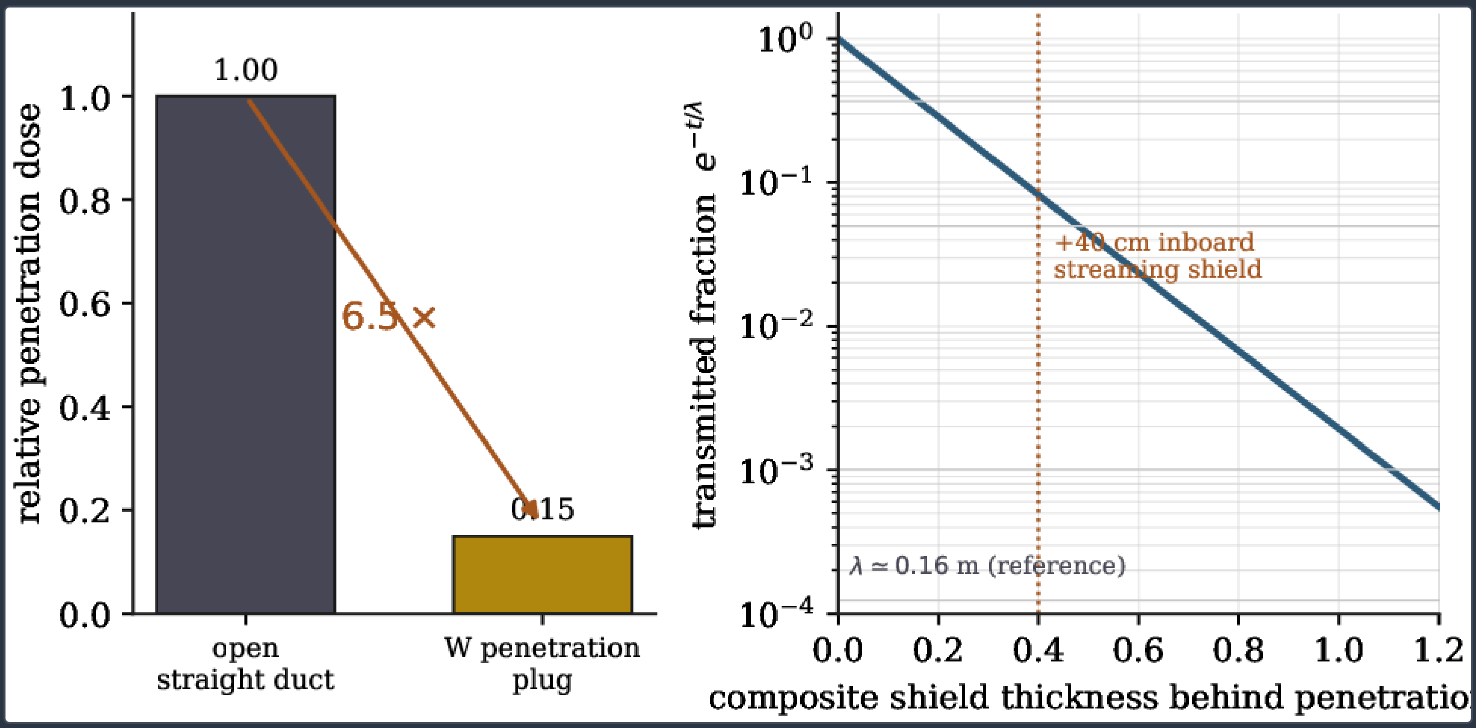


Left: a tungsten penetration plug in the widest (1.0 m) straight end duct returns $0.15\times$ the open-duct dose, a $6.5\times$ reduction (penetration-streaming Monte-Carlo study). Right: attenuation of the transmitted field behind the penetration with composite-shield thickness at a reference e-fold length $\lambda \simeq 0.16\,m$; the 40 cm inboard streaming shield marker corresponds to the beam-line dog-leg (BOM-06).

| QUANTITY | VALUE | SOURCE |
|---|---|---|
| **port-area budget** | $0.719\ m^2$ | BOM-06 |
| **port-area demand** | $0.720\ m^2$ | BOM-06 |
| **neutral-beam share of ports** | 67% | BOM-06 |
| **streaming TBR penalty (dog-leg + 40 cm shield)** | $-0.4\%$ $(0.742 \to 0.739)$ | BOM-06 |
| **net TBR, 3-D CAD with ports (single-null)** | 1.12 | BV-05B |
| **net TBR, 3-D CAD with ports (double-null)** | 1.07 | BV-05B |
| **tungsten-plug dose factor (1.0 m duct)** | $0.15\times$ $(6.5\times)$ | register |
| **reference attenuation e-fold $\lambda$** | 0.16 m | register |

Penetration-streaming and port summary.

## FIRST-WALL SPECTRUM AND THE R2S SOURCE TERM

The activation and dose calculation is normalized to the same design power. On the P3 three-dimensional OpenMC model the first-wall total neutron flux is 5.628e14 nps, of which 1.071e14 nps (19.0%) lies above 10 MeV and 17.1% falls in the 14 MeV source band; the breeder-zone flux is 1.302e14 nps (BR-L2-A23). An uncollided-current cross-check at the 1.89 MW/squarem wall load returns 8.390e13 nps, consistent with the tallied first-flight component (Figure 5), which verifies the multigroup condensation 19. These integrals are the spectral source term for the Bateman solve 10.

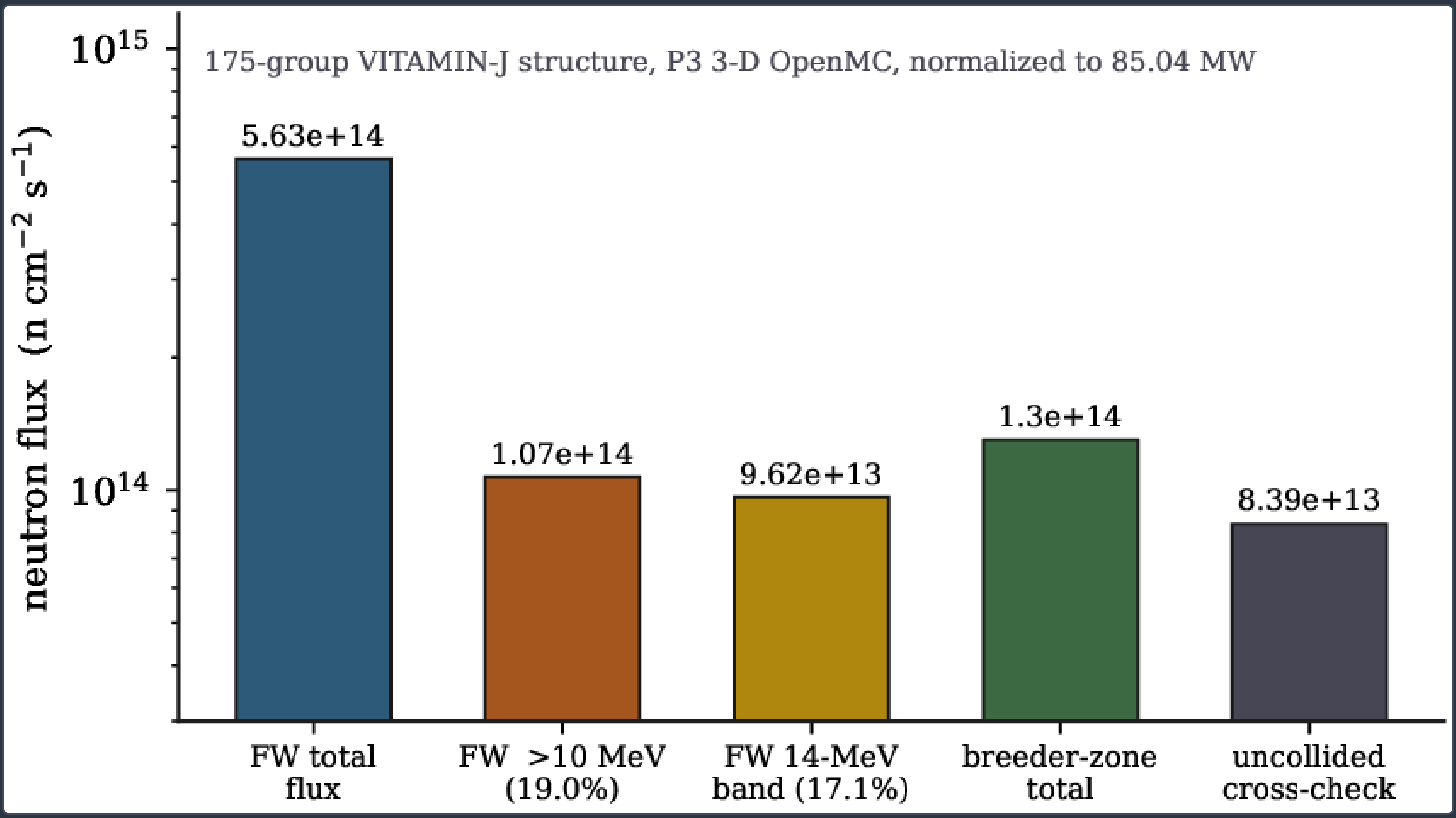


First-wall and breeder-zone spectral partition (175-group VITAMIN-J, P3 three-dimensional OpenMC, normalized to 85.04 MW; BR-L2-A23): first-wall total flux, its $> 10\ MeV$ and 14 MeV-band components, the breeder-zone total, and the uncollided-current cross-check.

## ACTIVATION INVENTORY, DECAY HEAT, AND WASTE CLASS

Feeding the group flux to ALARA over a one-full-power-year irradiation and cooling the two-zone slab (3 cm first wall of reduced-activation Eurofer-97, 50 cm breeder zone of Eurofer/beryllium/$Li_4SiO_4$ at 90% $^{6}Li$) gives the inventory of Table 3 and Figures 6–8. The first-wall specific activity 12 is 2.64e14 becquerel/kg at shutdown, decaying to 1.31e14 at one day, 9.37e13 at 100 days, 7.13e13 at one year and 2.70e7 becquerel/kg at 100 years; the shutdown field is dominated by short-lived $^{56}Mn$ and $^{52}V$, the day-to-year field by $^{55}Fe$, $^{54}Mn$, $^{51}Cr$ and $^{49}V$, and the century residue by $^{3}H$ and $^{53}Mn$. The first-wall decay heat 12 falls from 56.0 W/kg at shutdown to 2.99 at one day and 1.22 W/kg at one year (Figure 7); the breeder-zone activity and decay heat are comparable at shutdown (2.34e14 becquerel/kg, 29.2 W/kg) and its century-scale residue is entirely bred tritium held in the ceramic — an artifact of no-purge bookkeeping, since in operation tritium is the recovered product, not a waste term.

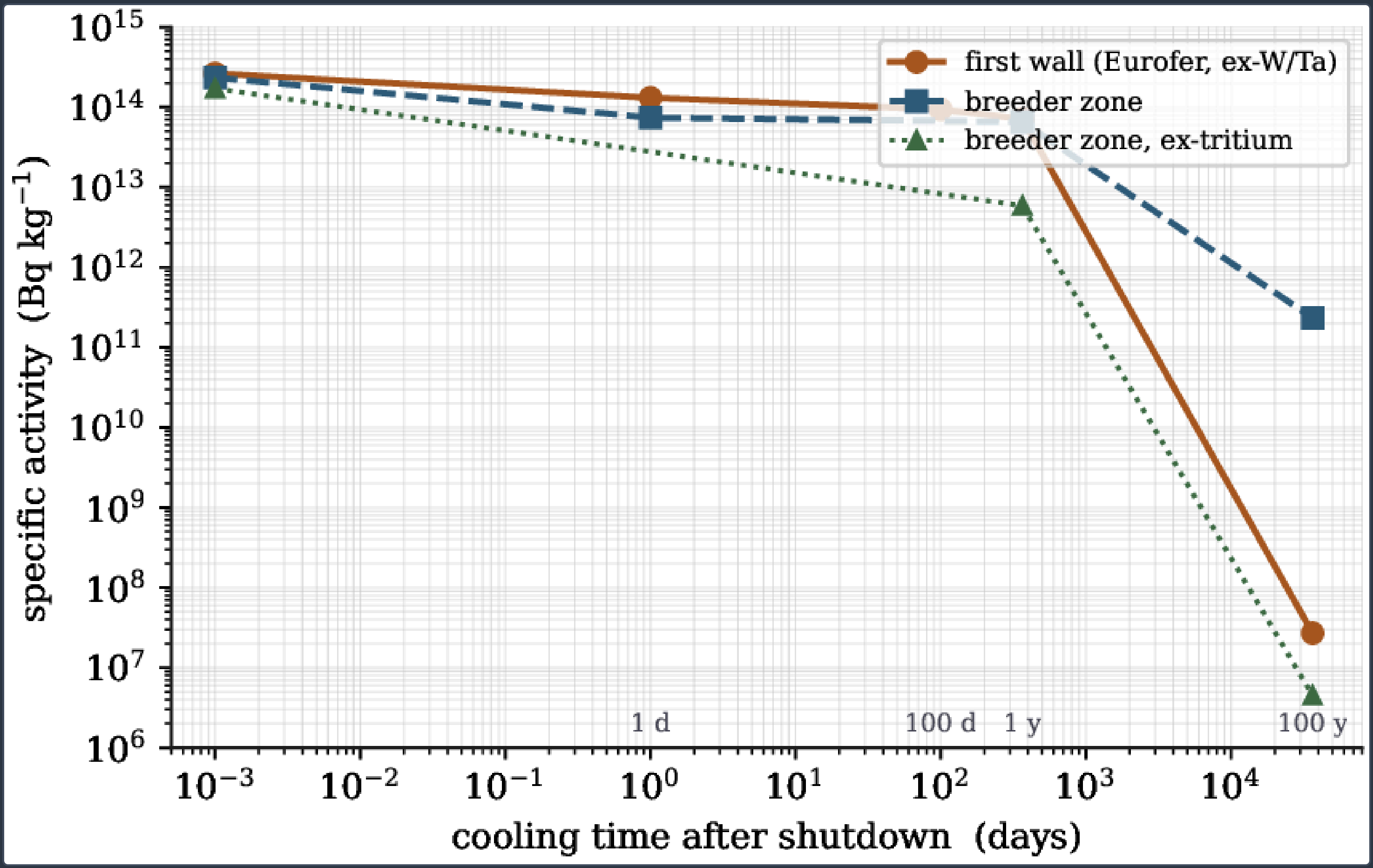


Specific activity versus cooling time for the first wall and breeder zone (BR-L2-A23). The breeder-zone century residue is bred tritium (no-purge bookkeeping); the ex-tritium curve shows the true structural residue.

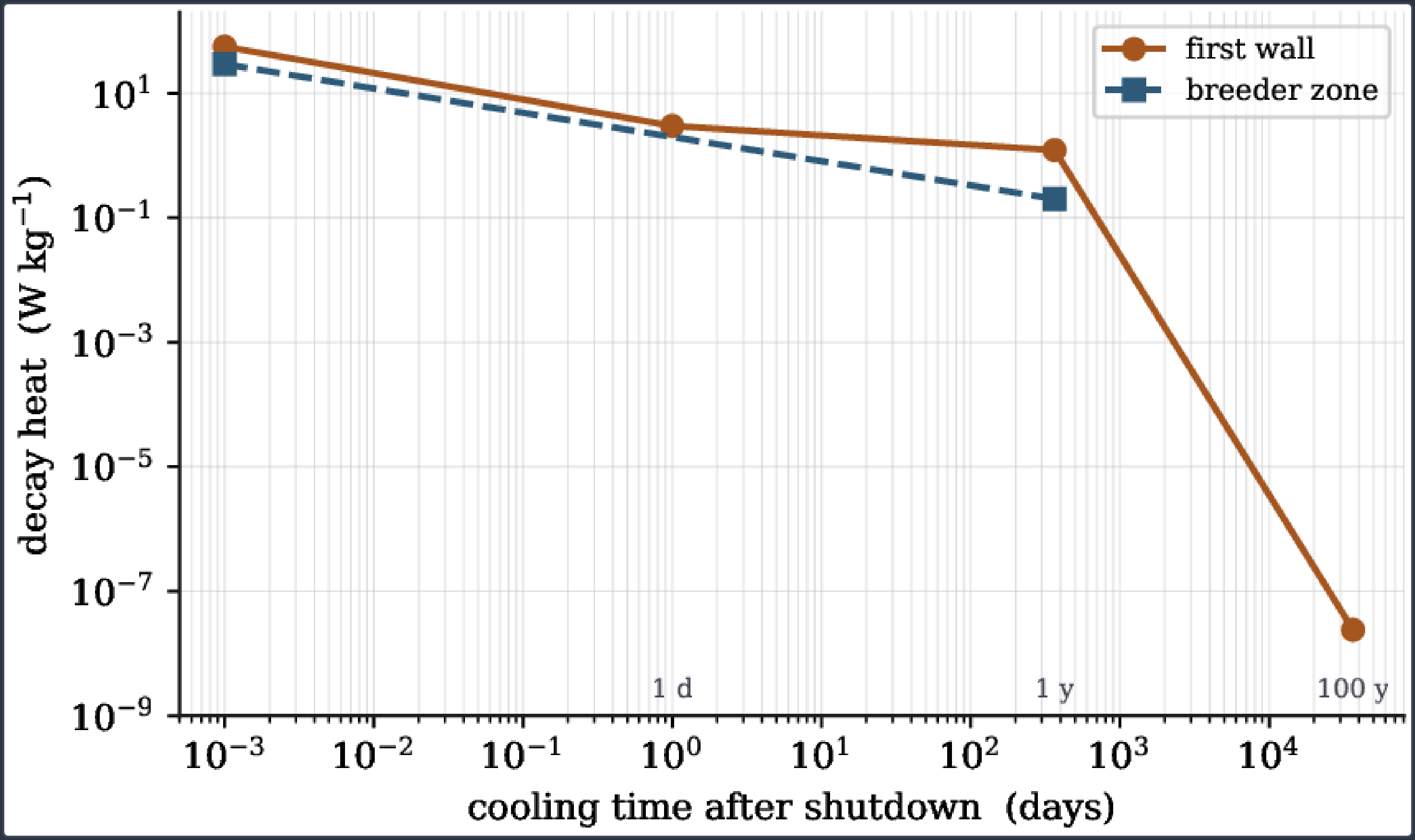


Decay heat versus cooling time for the first wall and breeder zone (BR-L2-A23). The first-wall decay heat falls below 1.3 W/kg within a year, setting the after-heat basis for the walk-away safety case.

The waste classification follows the NRC 10 CFR 61 concentration-ratio indices computed by ALARA (Figure 8). The Class-C index is $\leq 2.6e-3$ in *both* zones at *all* cooling times, driven by $^{14}$C — far below the Class-C boundary, so nothing is greater-than-Class-C and there is no long-lived driver in the modelled composition. The Class-A index is dominated by tritium (first-wall $2.52$, falling to 9.5e-3 at 100 years); once tritium is recovered the structure is Class-A low-level waste at discharge. Tritium management, not activation, sets the handling class.

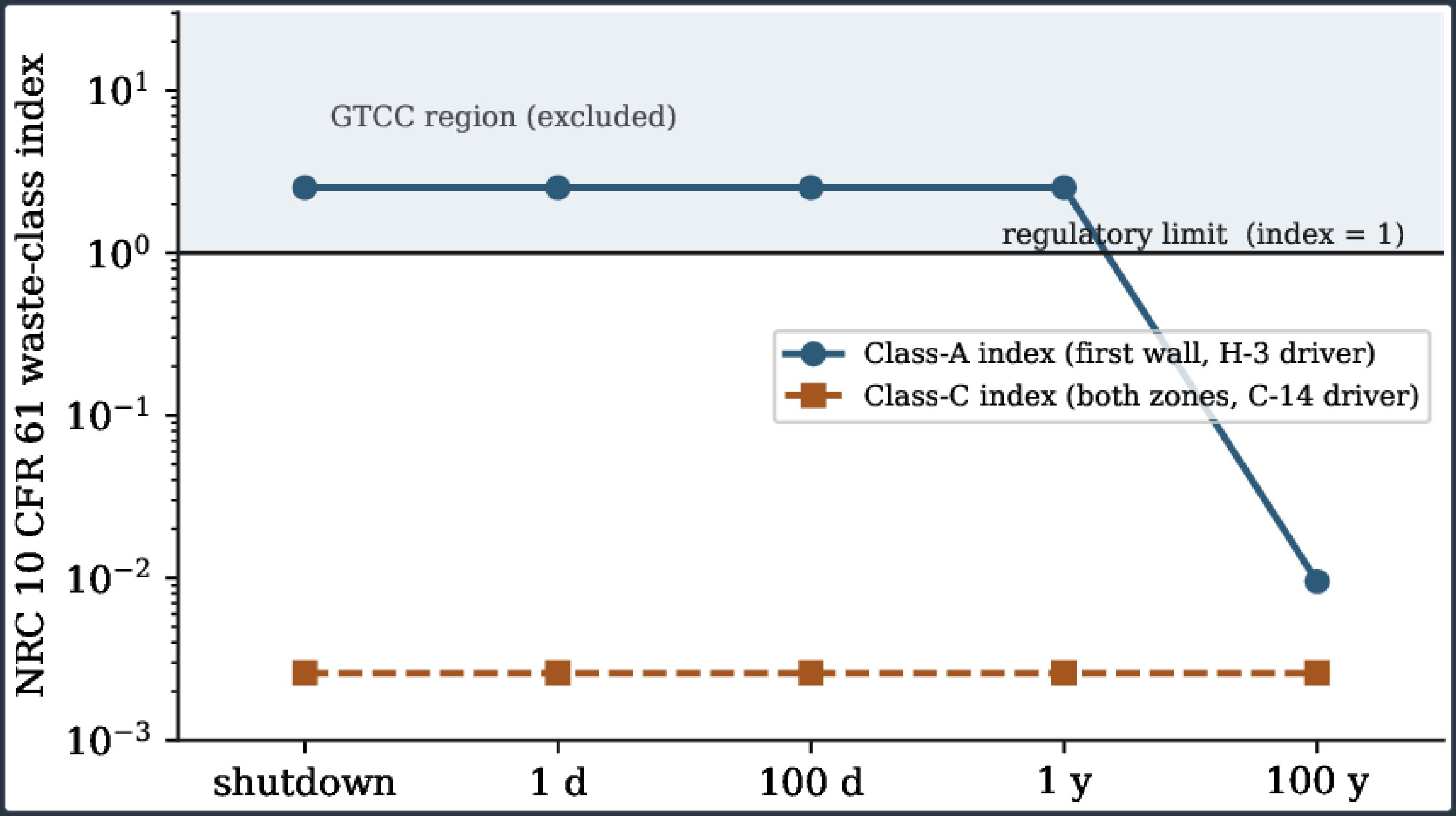


NRC 10 CFR 61 waste-class indices versus cooling time (BR-L2-A23): the Class-C index stays $\leq 2.6e-3$ in both zones at all times (nothing greater-than-Class-C), while the Class-A index is tritium-driven. The structure is low-level waste at discharge.

| QUANTITY | FIRST WALL | BREEDER ZONE | NOTE |
|---|---|---|---|
| **neutron flux (nps)** | 5.628e14 | 1.302e14 | VITAMIN-J tally |
| **specific activity, shutdown (becquerel/kg)** | 2.64e14 | 2.34e14 | $^{56}$Mn/$^{52}$V |
| **specific activity, 1 y (becquerel/kg)** | 7.13e13 | 6.55e13 | $^{55}$Fe/$^{54}$Mn |
| **specific activity, 100 y (becquerel/kg)** | 2.70e7 | 2.33e11 | $^{3}$H/$^{53}$Mn |
| **decay heat, shutdown (W/kg)** | 56.0 | 29.2 | |
| **decay heat, 1 y (W/kg)** | 1.22 | 0.20 | |
| **10 CFR 61 Class-C index** | $\leq 2.6e-3$ | $\leq 2.6e-3$ | $^{14}$C driver |
| **waste class at discharge** | 2cLLW (not GTCC) | tritium-managed | |

R2S activation inventory and waste class (BR-L2-A23; 1 full-power-year irradiation, 175-group VITAMIN-J, normalized to §I85.04

## THE RECEPTOR: FROM STREAMING SOURCE TO OCCUPATIONAL DOSE

The two halves of the account meet at the maintainer's location (Figure 9). The R2S decay-gamma source 13 is strongest in the activated first wall and blanket, but the field that actually reaches a maintenance position is filtered by the same penetration geometry that governed the neutron leakage: a receptor at the mouth of a bent, plugged and shielded duct sees the wall-albedo tail of 8 and 9, not the line-of-sight source. Because the neutron transport that built the inventory and the photon transport that delivers the dose share one CAD-faithful geometry, the occupational-dose estimate inherits the streaming mitigations directly rather than requiring a separate, decoupled shielding sum (Figure 10). This coherence — one geometry, one transport, from the streaming penetration through the activation to the receptor — is what makes the neutron-safety case auditable.

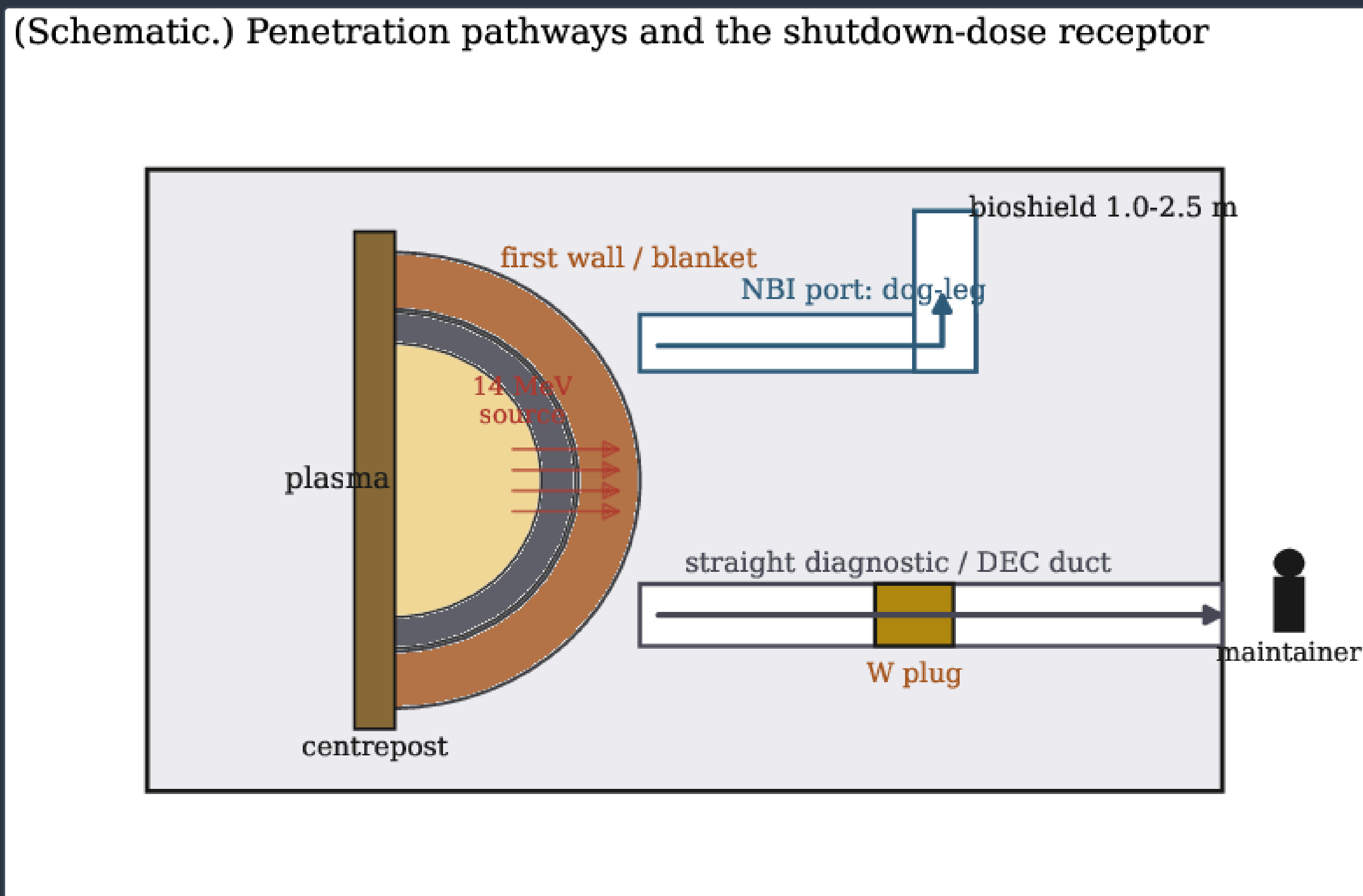


(Schematic.) Penetration pathways around the breeder: the beam-line dog-leg that breaks the neutron line of sight, the straight diagnostic/direct-conversion duct closed by a tungsten plug, the inboard streaming shield, and the bioshield behind which the maintainer stands. Not to scale.

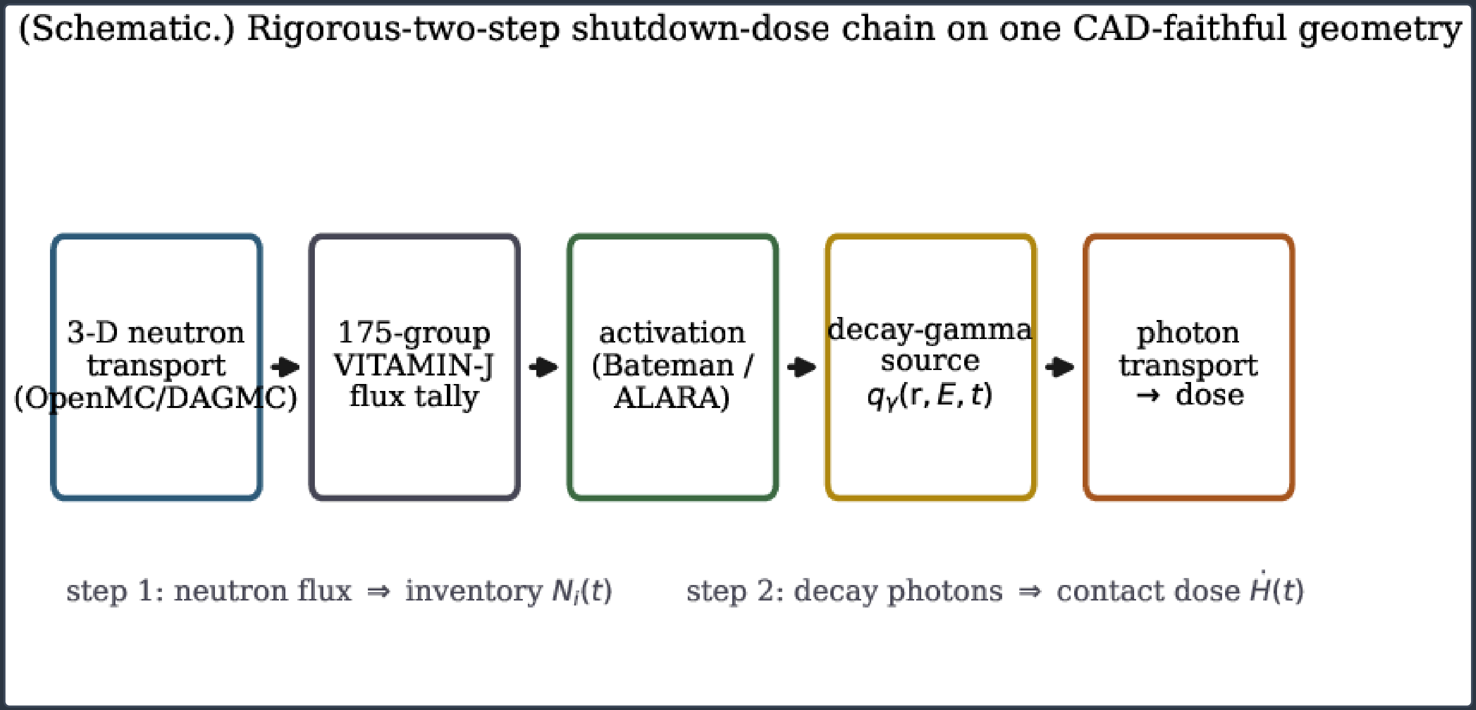


(Schematic.) The rigorous-two-step chain of Section 2: neutron transport fixes the 175-group flux, the Bateman/ALARA solve builds the activation inventory, and the decay-gamma source is transported back through the *same* CAD-faithful geometry to the receptor dose.

§ 6

# Discussion

## QUANTITATIVE COMPARISON WITH PUBLISHED PRACTICE

The streaming result sits squarely within established fusion-neutronics practice while being specific to a compact, thin-inboard-shield spherical tokamak. The $a^2/L^2$ line-of-sight law and the $\alpha^{-2}$ dog-leg suppression are the textbook results of duct-streaming theory [25,26,27], and the tungsten-plug factor of $\mathbf{0.15}\times$ ($\Sigma_t^p t_p \approx \mathbf{1.9}$ mean free paths) is consistent with the high-$Z$ plug attenuation used in ITER port and diagnostic-penetration shielding studies [15,14]. The need for adjoint-driven variance reduction to make the deep-streaming FOM 16 tolerable, and the choice of CADIS/FW-CADIS weight windows, follow the same reasoning that governs ITER-scale Monte-Carlo shielding [10,11,13]. Where the compact ST differs is in the *margin*: the port budget saturates at 0.719 m$^2$ with zero headroom (BOM-06), so the breeding penalty of penetration is not a small perturbation to be absorbed but a first-order design constraint — which is exactly why the with-ports TBR of $\mathbf{1.12}/\mathbf{1.07}$ (BV-05B), still above the 1.05 floor, is the load-bearing breeding number rather than the idealized $\mathbf{1.17}$.

## THE DOSE CASE IN CONTEXT

On the activation side, the first-wall specific activity of 2.64e14 becquerel/kg at shutdown and the decay heat of 56.0 W/kg are typical of a reduced-activation ferritic–martensitic first wall under 14 MeV loading [19,20], and the collapse of the Class-C index to $\leq \mathbf{2.6}e - \mathbf{3}$ places the structure firmly in the low-level-waste class, consistent with the fusion activated-material management literature [22]. The result that tritium management — not structural activation — sets the handling class is the same conclusion reached for helium-cooled ceramic-breeder blankets [21], and it is what allows the wider Kronos platform to argue a byproduct-material regulatory posture rather than a power-reactor one [38,37]. The shutdown-dose model reported here is the validated neutron-and-photon source term on which that occupational-safety and decommissioning case is built, and it connects directly to the neutronics-and-activation digital twin [33], the component-activation and waste-routing study [34], and the centrepost fluence-and-shielding life-limiter [35] that share this transport basis. The nuclear-data uncertainty that dominates the breeding error bar is treated separately [36].

§ 7

# Limitations

One honest gate remains. The R2S model resolves the activation-gamma source on the CAD-faithful geometry and the streaming factors on the analytic-plus-Monte-Carlo basis of Sections 2–5, but the *location-specific* occupational dose *rate* at each named maintenance position — the final $\dot{H}(r_0, t_c)$ of 14 at every workstation — is the staged product of the same DAGMC/OpenMC photon-transport step on the built layout, not a new toolchain. It is computed on the identical geometry and source term reported here; what remains is to enumerate the receptor positions of the final maintenance plan and tabulate the per-position rates. No new physics or code is required, only the frozen layout.

§ 8

# Conclusion

The Hyperion breeder's third-leg neutron account — the streaming penetrations, the breeding penalty they impose, and the occupational dose they set — is closed in three dimensions on CAD-faithful geometry. A 3.009e19 /s, 67.8 MW source drives a transport with a $0.121$ leakage fraction, a 7.0e14 nps first-wall flux and 74.6 MW of nuclear heating. The line-of-sight $a^2/L^2$ streaming law and its $\alpha^{-2}$ dog-leg suppression, derived here and confirmed by three-dimensional Monte-Carlo, explain why the port-saturated ($0.719$/0.720 m$^2$) layout holds its breeding penalty to $-0.4\%$ with a beam-line dog-leg and a 40 cm shield, and why a tungsten penetration plug ($6.5\times$ reduction) is the load-bearing mitigator of the one duct that cannot be bent. With those mitigations the net TBR with real ports settles at $1.12/1.07$, above the 1.05 floor. The rigorous-two-step model, built on the same geometry, gives a first-wall shutdown activity of 2.64e14 becquerel/kg decaying to 7.13e13 becquerel/kg at one year, a decay heat of $56.0 \rightarrow 1.22\,W/kg$, and a Class-C index $\leq 2.6e-3$ in both zones at all times — low-level waste, tritium-limited, nothing greater-than-Class-C. The account is complete, CAD-faithful and auditable end to end, from the streaming penetration to the maintainer's dose.

Acknowledgments tocsectionAcknowledgments Part of the Kronos Fusion Energy 2026 design series. The authors thank the Kronos de-risking campaign for the frozen neutronics, streaming and activation serials on which this work is grounded.

Reproducibility. The source term, transport balance, CAD-faithful chain, port budget and shutdown-dose spectra are frozen results in the Kronos Physics De-Risking Register (BR-OUT-3, BR-L1-A5, BR-L2-A22, BR-L2-A7b, BV-05B, BOM-06, BR-L2-A23, KX-L1-A3), regenerable from the archived OpenMC/DAGMC/ALARA decks with fixed seeds and recorded nuclear-data revisions. This paper is archived at doi:10.5281/zenodo.22645842; official version: https://www.kronosfusionenergy.com/publications/neutron-streaming-duct-and-port-penetrations-and-occupa.html and the register at doi:10.5281/zenodo.22133057; the figure-generation script that renders every data figure from the frozen numbers is deposited with this paper.

Data availability tocsectionData availability The neutron-balance, port-streaming, spectral and activation tables are archived with the deposit (doi:10.5281/zenodo.22645842) and reference the Kronos 2026 series. Any economic analysis is reported separately and is not part of the public deposit.

Competing interests tocsectionCompeting interests Provisional patent applications relating to aspects of this work have been filed.

APPARATUS

# *Portfolio, People & Record*

*The intellectual-property estate, the people who built it, the limitations that gate it, and the sources it rests on.*

| 1 | 4 | 40 | 27 |
| --- | --- | --- | --- |
| GRANTED PATENT | 2026 PROVISIONALS | TEAM MEMBERS | 2022 PROVISIONALS |

INTELLECTUAL PROPERTY

# The patent portfolio

The estate spans a granted high-field magnet patent, pending utility and 2026 provisional filings that map to the two products, a digital-twin control provisional, a registered trademark application, and the original 2022 provisional family. Every patentable disclosure in the five-paper arXiv drop was protected **before** publication: the breeder and burner provisionals were filed 1–2 August, and a publication-gap omnibus filing the evening before the drop swept up the DEC, plasma-control, and REBCO-winding matter of the three otherwise-unprotected papers. Patent numbers and application serials are matters of public record; claim scope is summarised, not reproduced.

## GRANTED & PENDING UTILITY

| | | |
|---|---|---|
| US 12,009,112 | High-field tilted graded-REBCO magnet architecture (KRONO-002A) · *app. 17/878,550* | GRANTED |
| US 17/878,507 | Core device / method (KRONO-001A) · *utility* | PENDING |

## 2026 PROVISIONAL FILINGS — MAPPED TO THE PRODUCTS

| | | |
|---|---|---|
| 64/124,209 | Hyperion — spherical-tokamak tritium / helium-3 foundry · *breeder · filed Aug 2026* | FILED |
| 64/124,220 | Aegis / MetroVolt — synchrotron-cutoff, fuel-selection & plug-winding · *generator · filed Aug 2026* | FILED |
| 64/115,167 | KRONOS-CTRL digital-twin plant control · *provisional · filed Jul 2026* | FILED |
| 64/005,440 | Integrated spherical-tokamak fusion architecture · *early integrated-architecture filing · filed Mar 2026* | FILED |
| 64/105,530 | Negative-triangularity spherical-tokamak architecture · *foundational ST filing · filed Jul 2026* | FILED |
| 64/128,097 | Publication-gap omnibus — quasineutral two-species expander DEC · provenance-gated / latency-split plasma control · as-built high-field winding & conductor architecture · *filed 7 Aug 2026, the evening before the arXiv drop* | FILED |

## TRADEMARK & ORIGIN

| | | |
|---|---|---|
| FTK-98801894 | Kronos Fusion Energy — trademark application | FILED |
| KR-2022-* | Original provisional family (KR-2022-00001 … 00027) · *27 filings, 2022* | PRIORITY |

The narrow, defensible magnet novelty — the specific conductor and the digital-twin winding optimisation, not high-field REBCO as a category — is the commercial core that can earn ahead of any Q > 1 milestone, with markets in fusion magnet supply, MRI/NMR, accelerators, and proton therapy. The claim is scoped honestly: the high field is a *system field* result, not a stand-alone-coil record; the small-bore plug coil is structurally infeasible as a bare winding but resolved by a stress-managed structural shield (feasible-pending-FEA); and the winding-tape experiment returned a *null result*. The value is the method, not a field record.

THE TEAM

# Founding partners, board, advisors & auditors

Kronos is built by a bench of advanced-fuel-fusion, high-field-magnet, direct-conversion, and materials specialists, with a board and operations team drawn from defense, national laboratories, and industry. Dates are shown as ranges; where a tenure has ended or is term-ending, the range says so.

## FOUNDING PARTNERS — SCIENCE

**Dr. Gerald Kulcinski**
Co-Founder · Helium-3 & Advanced-Fuel Fusion
*UW–Madison · 2023–Present*

**Dr. Carl Weggel**
Chief Scientist / S.M.A.R.T. Design
*MIT Alcator Program · 2022–Present*

**Dr. Robert J. Weggel**
Magnetic Field Design
*MIT Magnet Lab · 2022–Present*

## BOARD

**Priyanca Ford**
Founder & CEO · Executive Board
*2022–Present*

**Bandel Carano**
Finance / Strategy
*Oak Investment Partners / Stanford · 2025–2026*

**Patrick Schweiger**
Fusion Device Engineering
*Oklo / CFS / TerraPower · 2025–Present*

## SCIENTIFIC ADVISORS

**Dr. Steven O. Dean**
Fusion Policy & History
*DOE / Fusion Power Associates · 2025–Present*

**Dr. Patrick H. Diamond**
Plasma Turbulence & Transport
*UC San Diego · 2025–Present*

**Dr. Jack J. Dongarra**
HPC & Numerical Algorithms
*Turing Award · 2025–Present*

**Dr. Nasr M. Ghoniem**
Chief Material Scientist
*UCLA · 2025–Present*

**Dr. Siegfried Glenzer**
Plasma Physics & Laser Fusion
*Stanford / SLAC · 2022–Present*

**Dr. David A. Hammer**
Pulsed-Power Fusion
*Cornell · 2025–Present*

**Dr. Donald A. Spong**
Plasma Theory & Confinement
*ORNL · 2025–Present*

**Dr. Curtis Smith**
Risk Assessment & Nuclear PRA
*MIT / Idaho National Lab · 2025–Present*

**RADM (Ret.) David Goggins**
Naval Engineering & Power-Plant Design
*U.S. Navy · 2023–2026*

**Dr. Konstantin Batygin**
Mathematician
*Caltech · 2022–2025*

**Dr. Ruben Fair**
Magnet Design / ITER Liaison
*PPPL / Jefferson Lab · 2022–2025*

**Dr. Paul S. Weiss**
Materials & Nanotechnology
*UCLA · 2022–2025*

## SCIENTIFIC AUDITORS

**Dr. Wilfred A. Cooper**
Plasma Equilibrium Theory
*EPFL / Swiss Plasma Center · 2025–Present*

**Dr. Ahmed Hassanein**
Plasma–Material Interactions
*Purdue / Argonne · 2025–Present*

**Dr. Patrick E. Hopkins**
Extreme Thermal Materials
*U. of Virginia · 2025–Present*

**Dr. Peter Hosemann**
Materials Joining & Structural Integrity
*UC Berkeley · 2025–Present*

**Dr. Travis W. Knight**
Advanced Nuclear Fuels & Systems
*U. of South Carolina · 2025–Present*

**Dr. Philippe Lebrun**
Cryogenics & Magnet Cooling
*CERN · 2025–Present*

**Dr. Nitendra Singh**
Nuclear Safety & Fuel Cycle
*ITER · 2025–Present*

**Dr. Guido Van Oost**
Magnetic Confinement & Fusion Systems
*Ghent University · 2025–Present*

**Dr. Gary S. Was**
Radiation Materials & Structural Integrity
*U. of Michigan · 2025–Present*

**Dr. Ray Sedwick**
Direct Energy Conversion
*U. of Maryland · 2025*

## OPERATIONS

**Michael Laughlin**
Chief Operating Officer
*2022–Present*

**Martin Owens**
Chief Strategy Officer
*LANL / GE Hitachi · 2022–Present*

**MG (Ret.) Paul Pardew**
Chief Contracting Officer
*Army Contracting Command · 2022–Present*

**David Beck**
Fusion Commercialization
*U.S. Space Force · 2024–Present*

**Sushma Bhatia**
Environmental & Legislative
*Google · 2022–Present*

**Michael De Frenza**
Technology Licensing
*2023–Present*

**MG (Ret.) Robin L. Fontes**
Cybersecurity & Defense
*Army Cyber Command · 2022–Present*

**Vijay Gehani**
Supply Chain & Components
*INOX India · 2024–Present*

**Jon Michel Greenwood**
IT & AI Infrastructure
*Live Nation · 2023–Present*

**Brian C. O'Neill**
National Security
*CIA / ODNI · 2022–Present*

**Gen. (Ret.) Gustave F. Perna**
DoD Liaison
*Operation Warp Speed · 2022–2023*

**Andrea Romero**
Marketing Lead
*2022–Present*

Legal counsel is retained; those roles are held on the internal roster and are not listed here.

SOURCES

# References


1 J E Menard *et al*, Fusion nuclear science facilities and pilot plants based on the spherical tokamak, *Nucl. Fusion* **56** 106023 (2016). doi:10.1088/0029-5515/56/10/106023

2 B N Sorbom *et al*, ARC: a compact, high-field, fusion nuclear science facility and demonstration power plant with demountable magnets, *Fusion Eng. Des.* **100** 378 (2015). doi:10.1016/j.fusengdes.2015.07.008

3 A J Creely *et al*, Overview of the SPARC tokamak, *J. Plasma Phys.* **86** 865860502 (2020). doi:10.1017/S0022377820001257

4 M E Austin *et al*, Achievement of reactor-relevant performance in negative triangularity shape in the DIII-D tokamak, *Phys. Rev. Lett.* **122** 115001 (2019). doi:10.1103/PhysRevLett.122.115001

5 A Marinoni, O Sauter and S Coda, A brief history of negative triangularity tokamak plasmas, *Rev. Mod. Plasma Phys.* **5** 6 (2021). doi:10.1007/s41614-021-00054-0

6 P K Romano, N E Horelik, B R Herman, A G Nelson, B Forget and K Smith, OpenMC: a state-of-the-art Monte Carlo code for research and development, *Ann. Nucl. Energy* **82** 90 (2015). doi:10.1016/j.anucene.2014.07.048

7 D A Brown *et al*, ENDF/B-VIII.0: the 8th major release of the nuclear reaction data library with CIELO-project cross sections, *Nucl. Data Sheets* **148** 1 (2018). doi:10.1016/j.nds.2018.02.001

8 P P H Wilson, T J Tautges, J A Kraftcheck, B M Smith and D L Henderson, Acceleration techniques for the direct use of CAD-based geometry in fusion neutronics analysis, *Fusion Eng. Des.* **85** 1759 (2010). doi:10.1016/j.fusengdes.2010.05.030

9 J Shimwell *et al*, The Paramak: automated parametric geometry construction for fusion reactor designs, *F1000Research* **10** 27 (2021). doi:10.12688/f1000research.28224.1

10 J C Wagner and A Haghighat, Automated variance reduction of Monte Carlo shielding calculations using the discrete ordinates adjoint function, *Nucl. Sci. Eng.* **128** 186 (1998). doi:10.13182/NSE98-2

11 J C Wagner, D E Peplow and S W Mosher, FW-CADIS method for global and regional variance reduction of Monte Carlo radiation transport calculations, *Nucl. Sci. Eng.* **176** 37 (2014). doi:10.13182/NSE12-33

12 M A Cooper and E W Larsen, Automated weight windows for global Monte Carlo particle transport calculations, *Nucl. Sci. Eng.* **137** 1 (2001). doi:10.13182/NSE00-34

13 A Davis and A Turner, Comparison of global variance reduction techniques for Monte Carlo radiation transport simulations of ITER, *Fusion Eng. Des.* **86** 2698 (2011). doi:10.1016/j.fusengdes.2011.01.059

14 Y Chen and U Fischer, Rigorous MCNP based shutdown dose rate calculations: computational scheme, verification calculations and application to ITER, *Fusion Eng. Des.* **63–64** 107 (2002). doi:10.1016/S0920-3796(02)00144-8

15 A Turner and Z Ghani, Nuclear analysis and shielding optimisation in support of the ITER In-Vessel Viewing System design, *Fusion Eng. Des.* **89** 2080 (2014). doi:10.1016/j.fusengdes.2014.01.066

16 P Sauvan *et al*, Development of the R2SUNED code system for shutdown dose rate calculations, *IEEE Trans. Nucl. Sci.* **67** 1213 (2020).

17 P P H Wilson and D L Henderson, *ALARA: Analytic and Laplacian Adaptive Radioactivity Analysis*, University of Wisconsin Fusion Technology Institute report UWFDM-1070 (1998).

18 J-Ch Sublet, J W Eastwood, J G Morgan, M R Gilbert, M Fleming and W Arter, FISPACT-II: an advanced simulation system for activation, transmutation and material modelling, *Nucl. Data Sheets* **139** 77 (2017). doi:10.1016/j.nds.2017.01.002

19 R Lindau *et al*, Present development status of EUROFER and ODS-EUROFER for application in blanket concepts, *Fusion Eng. Des.* **75–79** 989 (2005). doi:10.1016/j.fusengdes.2005.06.186

20 M Abdou *et al*, Blanket/first wall challenges and required R&D on the pathway to DEMO, *Fusion Eng. Des.* **100** 2 (2015). doi:10.1016/j.fusengdes.2015.07.021

21 A Del Nevo *et al*, WCLL breeding blanket design and integration for DEMO 2015: status and perspectives, *Fusion Eng. Des.* **124** 682 (2017). doi:10.1016/j.fusengdes.2017.03.020

COLOPHON

# How this document was made

*The Kronos Fleet — Combined Editorial, 2026* is set in **Fraunces** (display), **Gelasio** (text), and **IBM Plex Mono** (data & equations), carried forward from the Kronos editorial design system.

The figures are rendered at 300 dpi from the deposited generator scripts; the document is composed as a single self-contained file with embedded fonts and imagery, paginated to US Letter, and rendered to PDF through a headless Chromium engine in matched light and dark editions.

Every headline quantity carries an evidence class; withdrawn and restated values are marked as such. Nothing herein is frozen beyond the founder-approved Tier-A set.

Explore it live — turn the interactive 3-D model, run the deposited solvers in the physics validator, and watch the companion film series.

LEGAL NOTICE

# Notice, status, and distribution

**Conceptual design & simulation study.** This document reports a conceptual design and simulation study. It is not a construction commitment, a safety-analysis report, a regulatory filing, or an offer of securities. Forward-looking statements — schedules, costs, market sizes, and performance — are estimates subject to the limitations set out in the Simulations part and may change.

**Numbers and their classes.** Quantities are reported with evidence classes and case labels; modelled, assumed, and requirement-class values are identified as such and are not to be quoted without their labels.

**Public edition.** This edition carries the physics and design only; all financial, funding, and defense-commercial content has been removed for public distribution. The scientific text corresponds to the arXiv and journal submissions.

THE 2026 KRONOS SERIES

# One programme, many papers

This editorial is one paper in the Kronos 2026 series — a real fusion company's complete, reproducible physics record for a spherical-tokamak breeder and its low-neutron D–$^3$He tandem-mirror burners. Every headline number is a frozen anchor in the Physics De-Risking Register.

Explore the whole programme: the De-Risking Register, the interactive 3-D model, and the physics validator.

KRONOS FUSION ENERGY

# *Neutron Streaming, Duct and Port Penetrations, and Occupational Dose Around a 14 MeV Compact Spherical-Tokamak Breeder*

A real fusion company building real machines. Explore the science, live.

Zenodo · doi:10.5281/zenodo.22645842

Read on kronosfusionenergy.com

The Physics De-Risking Register